

Dynamical systems with multiple long-delayed feedbacks: Multiscale analysis and spatiotemporal equivalence

Serhiy Yanchuk¹ and Giovanni Giacomelli²

¹*Weierstrass Institute for Applied Analysis and Stochastics, Mohrenstrasse 39, 10117 Berlin, Germany*

²*CNR–Istituto dei Sistemi Complessi–via Madonna del Piano 10, I-50019 Sesto Fiorentino (FI), Italy*

(Received 10 June 2015; published 2 October 2015)

Dynamical systems with multiple, hierarchically long-delayed feedback are introduced and studied extending our previous work [Yanchuk and Giacomelli, *Phys. Rev. Lett.* **112**, 174103 (2014)]. Focusing on the phenomenological model of a Stuart-Landau oscillator with two feedbacks, we show the multiscale properties of its dynamics and demonstrate them by means of a space-time representation. For sufficiently long delays, we derive a normal form describing the system close to the destabilization. The space and temporal variables, which are involved in the space-time representation, correspond to suitable time scales of the original system. The physical meaning of the results, together with the interpretation of the description at different scales, is presented and discussed. In particular, it is shown how this representation uncovers hidden multiscale patterns such as spirals or spatiotemporal chaos. The effect of the delay size and the features of the transition between small and large delays is also analyzed. Finally, we comment on the application of the method and on its extension to an arbitrary, but finite, number of delayed feedback terms.

DOI: [10.1103/PhysRevE.92.042903](https://doi.org/10.1103/PhysRevE.92.042903)

PACS number(s): 89.75.Kd, 02.30.Ks, 05.45.–a

I. INTRODUCTION

Complex networks are one of the main subjects of the current research on dynamical systems. As part of this research, it has become necessary to address delayed interactions. In fact, due to the finite propagation velocity of the information, additional time scales can be introduced that are typically comparable to or higher than the intrinsic time scales of the connected systems. Time delay effects [1] are reported in fields such as laser physics [2–5], vehicle systems [6], neural networks [7], and information processing [8], mainly in the case of the action of a single delayed feedback.

The specific feature of delay dynamical systems is that the corresponding phase space is infinite-dimensional [9]: in order to solve the model equations, the state of the system on a time interval equal to the delay τ has to be provided as initial conditions. On the other hand, it has been shown that the dimension of attractors in delay dynamical systems is finite and it may scale linearly with τ [10]; moreover, a part of the spectrum of Lyapunov exponents approaches a continuous limit for a long delay [11–15]. The latter case is of particular interest, as it indicates that many features of high-dimensional phenomena are expected to occur, and indeed spatiotemporal chaos [16], square waves [1,17], Eckhaus instability [18], coarsening [4], and nucleation [19] have been observed.

In the above-mentioned situations, the inspection of the dynamics reveals the existence of many different, well-separated time scales. This allowed a suitable representation to be built in which the delay time can be interpreted as the size of a one-dimensional, spatially extended system [16,17,20–25], and it explains new phenomena [4,18,19,26–28]. New challenging problems arise in the general case of a system with several delayed feedbacks, especially when the delays are acting on different time scales [29].

In this work, we concentrate on the case of multiple, hierarchically long delays. In such a configuration, the temporal dynamics shows a rich structure that can be meaningfully understood by means of suitable representations. Furthermore,

complex patterning in the time domain results in simple structures in the new framework. In particular, we focus on a two-delay model and its multiscale analysis. Nevertheless, as discussed below, we expect that the dynamical behavior in more complicated cases would be similar, as it will contribute on different scales, each with specific features.

This paper extends our previous article [29], detailing the three-dimensional spatiotemporal representation of the dynamics of the delayed system with two delays. Moreover, we present an analysis of the correlations on different time scales and a complete derivation of the normal form equations, as was recently outlined in Ref. [29]. The effects of the boundary conditions and the study of the transition from small to large delays are also analyzed extensively, together with a discussion of the case of multiple delays.

The paper is organized as follows. In Sec. II we introduce the two-feedback model and report some phenomenology from the numerical integration of it. The multiscale features of the dynamics are pointed out, and a spatiotemporal representation is schematized. We outline in Sec. III the details of the normal form derivation for the model. In Sec. IV we analyze the transition from small to large delays, while in Sec. V the extension to a higher number of delayed feedbacks is considered. Finally, in Sec. VI we draw our conclusions.

II. A MULTIPLE FEEDBACK MODEL: THE TWO-DELAY CASE

We consider the Stuart-Landau model (describing the Andronov-Hopf bifurcation) for an oscillatory instability, with two delayed feedback terms acting on the hierarchically long time scales $1 \ll \tau_1 \ll \tau_2$:

$$\dot{z} = az + bz_{\tau_1} + cz_{\tau_2} + dz|z|^2. \quad (1)$$

Here, the variable $z(t)$ is complex, the delayed terms are $z_{\tau_1} = z(t - \tau_1)$ and $z_{\tau_2} = z(t - \tau_2)$, and the parameters a , b , and c determine the instantaneous, τ_1 -, and τ_2 -feedback rates,

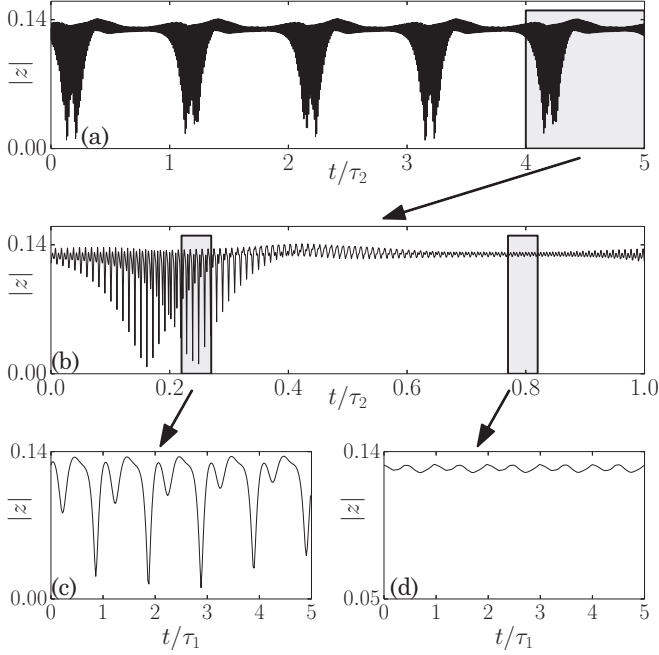


FIG. 1. Time series of $|z(t)|$ from (1), shown at different levels of zoom. Time is measured in units of τ_2 in (a) and (b) and in units of τ_1 in (c) and (d). The parameter values are $a = -0.985$, $b = 0.4$, $c = 0.6$ (corresponding to $P = 0.015$), $d = -0.75 + i$, $\tau_1 = 100$, and $\tau_2 = 10000$. Initial conditions are chosen randomly.

respectively. Using appropriate scaling transformations of the variable z , the parameter a can be made real and $d = -\mu + i$ with $\mu > 0$. For $\mu < 0$, the nonlinear term becomes expanding and the system no longer describes realistic bounded motions.

In Figs. 1 and 2, we show the results of the numerical integration of Eq. (1) for two different parameter choices. In Fig. 1, the time series of the variable $|z|$ exhibit “almost” periodic oscillations, with a period on the order of the delay time τ_2 [see Fig. 1(a)]. However, zooming into a time delay τ_2 interval [Fig. 1(b)], complex temporal structures are visible on a time scale τ_1 [Figs. 1(c) and 1(d)]. The same occurs for the parameters used in the simulation reported in Fig. 2. In this case, however, the dynamics is much more complicated at every scale, with large fluctuations of the amplitude.

A. Spatiotemporal representation of the dynamics

To disclose the hidden features of long-delayed dynamical systems with a single delay, a *spatiotemporal* representation (STR) has been introduced [16,20]. In this approach, the temporal variable t is parametrized by two new variables $\{\sigma, \theta\}$, playing the role of the *pseudospace* and *pseudotime*, respectively:

$$t = \sigma + \theta\tau, \quad (2)$$

where τ is the delay time. The representation (2) is a unique map from t on (σ, θ) if it is additionally assumed that $0 < \sigma \leq \tau$, and $\theta = 0, 1, 2, \dots$ is numbering the delay intervals. That is, $\sigma = t \bmod \tau$, and $\theta = [t/\tau]$ with $[\cdot]$ denoting the integer part. Accordingly, a temporal sequence is cut in slices of length τ : the variable spanning a single (delay)

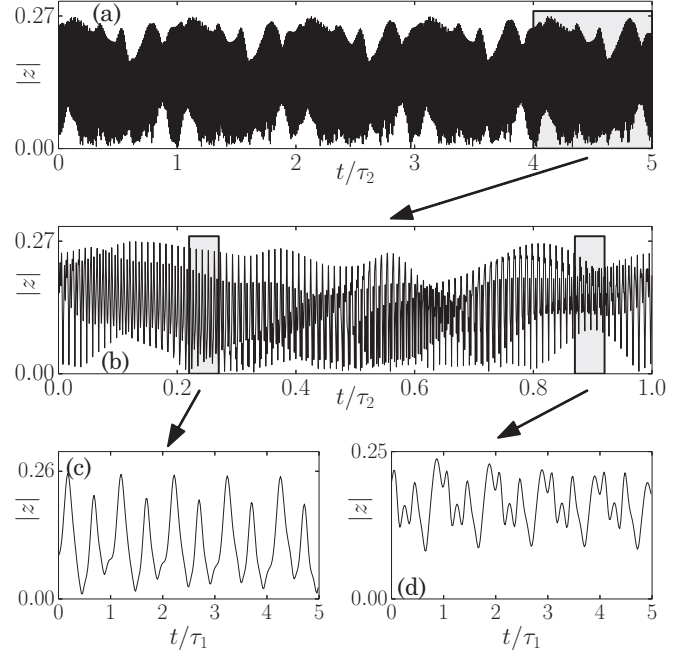


FIG. 2. Same as in Fig. 1 for $d = -0.1 + i$.

cell is the pseudospace σ , while the index numbering the slices is the pseudotime θ . The STR allows for a meaningful description of the dynamics observed both in experimental [4] and theoretical [16,19,26,30] setups.

As discussed in Ref. [20], the STR is very helpful in the visualization of some peculiar features of the dynamics of delayed systems. In particular, when the delay is larger than the typical time scales of the system without feedback, the system behavior is mainly determined by a local coupling in the STR coordinates.

The STR for systems with multiple, hierarchically long-delayed feedbacks can be generalized as

$$t = \sigma + n_1\tau_1 + n_2\tau_2 + \dots + n_{N-1}\tau_{N-1} + \Theta\tau_N, \quad (3)$$

where $1 \ll \tau_1 \ll \tau_2 \ll \dots \ll \tau_N$. Here, similarly, one assumes that $0 \leq \sigma \leq \tau_1$ and $0 \leq n_j \leq [\tau_{j+1}/\tau_j]$. We notice that σ and the n 's play the role of pseudospace variables, and Θ of the pseudotime variable. A more detailed discussion and explanation of the variables σ , n_j , and Θ will be given in Sec. V, where rescaled pseudospacial variables are introduced.

Another explicit introduction of the multiscale variables can be done as follows: $T_j = \mu_j t$, $j = 0, \dots, N$, where $\mu_j = 1/\tau_j \ll 1$ are small parameters such that $\mu_{j+1} \ll \mu_j$. In this case, the new time scale T_j is the time scale induced by the delay τ_j . Such an explicit introduction of the time-scale variables is equivalent to the one given by (3) in the sense that

$$n_j = \left\lfloor \frac{t \bmod \tau_{j+1}}{\tau_j} \right\rfloor = \left\lfloor T_j \bmod \frac{\tau_{j+1}}{\tau_j} \right\rfloor = [T_j]$$

when T_j is considered on a large interval from 0 to τ_{j+1}/τ_j . The explicit introduction of the time scales will be used in Sec. III for the derivation of the spatiotemporal model.

In the present case, with the use of STR with two delays, we obtain a 2D pseudospacial pattern (snapshot) that evolves

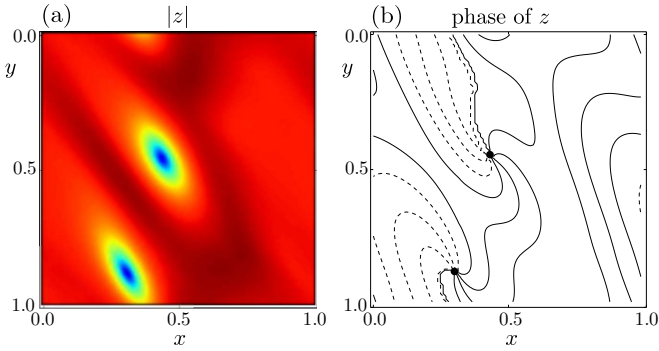


FIG. 3. (Color online) Spatiotemporal representation (see text) of the dynamics of system (1) in Fig. 1: spiral defects. (a) Snapshot of the spatial profile in the pseudospace coordinates (x, y) , plotted for $\theta_0 = 0.4$. (b) Constant level lines for the phase of z ; the circles denote the positions of defects. The phase is considered in the range $[-\pi, \pi]$, and the levels for negative and positive phases are shown as the dashed and solid lines, respectively. The spatial coordinates x and y are different time scales given by Eq. (37).

in pseudotime. An example, in Figs. 3 and 4, we plot two snapshots of the system (1) for the sets of parameters corresponding to Figs. 1 and 2, respectively. The definition of the pseudospacial variables (x, y) will be given in the following; here we anticipate that they are related to specific time scales of the original time series.

As seen in the pictures, the complex temporal dynamics of Figs. 1 and 2 uncovers in fact a deeper structure. The points with almost zero amplitude and τ_1 and τ_2 periodicity of Fig. 1 correspond to the cores of spiral (topological) defects of the 2D pattern [Fig. 3(a)], as confirmed by the analysis of the contour plot for the phase [see Fig. 3(b)]. In Fig. 4, an even more complicated temporal structure encodes a regime of 2D defect turbulence, with random creation, motion, and annihilation of topological defects. The observed patterns both change smoothly in time.

B. Multiscale dynamics

We return to the case of two delays (1). The phenomenology reported in the previous subsection indicates that the dynamics

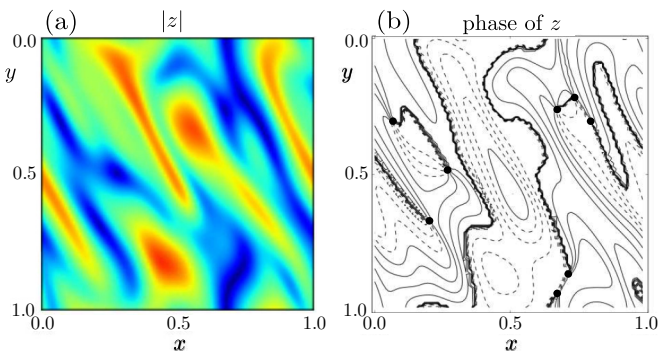


FIG. 4. (Color online) Spatiotemporal representation (see text) of the system dynamics in Fig. 2: defects turbulence. Plots are as in Fig. 3. The jumps of the phase from $-\pi$ to π are emphasized by thicker lines.

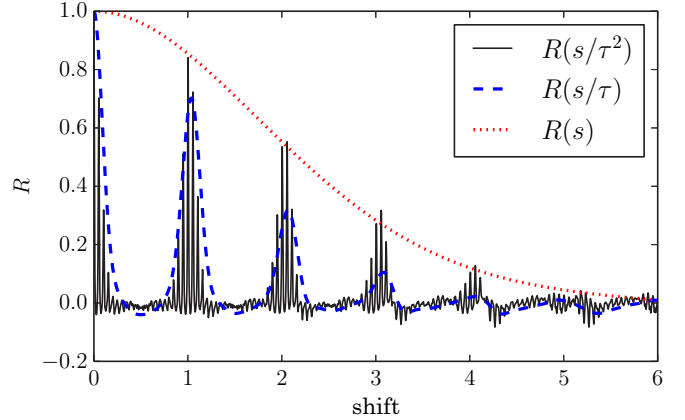


FIG. 5. (Color online) Autocorrelation function R of z for the solution of Eq. (2) with $a = -0.625$, $b = 0.4$, $c = 0.225$, $d = -0.1 + i$, $\tau_1 = \tau = 20$, and $\tau_2 = \tau^2 = 400$. R is plotted using three different rescalings for the shift (see inset).

of system (1) is strongly affected by the two time scales induced by the delayed feedbacks. A more quantitative analysis can be carried out on the time series by means of the (normalized) autocorrelation function

$$R(s) = \frac{\langle [|z(t-s) - \mu][|z(t) - \mu]| \rangle_t}{\sigma^2(|z|)}, \quad (4)$$

where $\langle \cdot \rangle_t$ denotes the time average, $\mu = \langle |z(t)| \rangle_t$, and $\sigma^2(|z|) = \langle (|z| - \mu)^2 \rangle_t$ are the average and the variance of the intensity. As shown in Ref. [31] for the single delay case, the autocorrelation function structure can be derived for a linear model with delay, and it obeys the very same equation. Moreover, a comparison with experimental and numerical results indicated that even such a simple approach is able to reproduce the findings in the case of more complicated dynamics with nonlinear terms. It is expected, therefore, that most of the features of the signal itself (such as the multiscale properties) are shared by the autocorrelation, even in the multiple delays case. As an example, the spatiotemporal representation for the autocorrelation was shown experimentally in Ref. [32] for a single delay, evidencing a multiscale structure and the existence of a drift.

In our case, we report in Fig. 5 the typical behavior of R for the time series of (1) for time delays $\tau_1 = \tau = 20$, $\tau_2 = \tau^2 = 400$, and the other parameter values as indicated in the figure. The solution at these parameter values corresponds to spatiotemporal chaos, as shown in Fig. 2. The autocorrelation R is shown as a function of different rescaled temporal shifts. When plotted in units of τ_2 (black, continuous line), a strong decay is visible within a τ_2 cell as a signature of the chaotic nature of the solution. However, the autocorrelation displays revivals at multiples of τ_2 , indicating that there is a coherence between the points at t and $\approx t - \tau_2$, or, in terms of the spatiotemporal coordinates (3), this is a high coherence between the same points in the pseudospace with fixed σ_0 and n_1 , and which are close in the pseudotime, i.e., n_2 and $n_2 - 1$.

When R is displayed in units of τ_1 (blue, dashed line), the fine structure of the first peak at the previous resolution is shown to reveal many peaks corresponding to multiples of τ_1 . Those multiple revivals, decaying within a τ_2 interval, indicate

that a τ_1 -long pattern is roughly coherent over some units. Analogously to the case with τ_2 , this implies the coherence between the points corresponding to the same σ_0 and n_2 but neighboring values of n_1 . The high correlation along the coordinates n_1 and n_2 implies that the solution changes slowly along them, thus allowing a pseudocontinuous description as a 2D spatial pattern with respect to the spatial coordinates σ_0 and n_1 and temporal coordinate n_2 . Finally, the autocorrelation displays a strong decay (red, dotted line) when plotted without rescaling (the unit is 1), characterizing the degree of disorder within a single τ_1 unit.

As seen from the Fig. 5, the decay rate of the peak envelope in the above scalings is of the same order. As a consequence, the dynamical properties of the system (e.g., coherence length) as a function of the corresponding rescaled variables are of comparable magnitude. This is a strong indication that the system can be effectively treated by means of a multiscale analysis, i.e., there exists a representation of the dynamics in terms of suitable variables where the behavior is evolving on a scale $O(1)$.

III. TOWARD A SPATIOTEMPORAL MODEL

In the previous section, we presented the results of a numerical integration of system (1). A close similarity to the dynamics of a spatially extended system is found when the STR is used to represent the results with suitable pseudospacial and temporal variables. As a further indication, the analysis of the autocorrelation function suggests that important features of the dynamics are connected to specific time scales of the time series, thus paving the way for a more rigorous approach based on a multiscale expansion of the model. As a consequence, we expect to obtain a spatiotemporal normal form in terms of suitable spacelike and temporal-like variables related to the above time scales.

As a first step toward the derivation of the normal form from the model (1), we study the properties of the destabilization of the steady state $z = 0$.

A. Destabilization and spectrum of the steady state

The long time delays τ_1 and τ_2 can be written as $\tau_1 = 1/\varepsilon$ and $\tau_2 = \kappa/\varepsilon^2$ with positive parameters ε and κ . Considering ε as a small parameter $\varepsilon \ll 1$, the scale separation $1 \ll \tau_1 \ll \tau_2$ is satisfied. The parameter κ is considered to be of order 1. Note that in the case of more than two delays on different time scales, one can proceed similarly and introduce the scaling $\tau_n = \kappa_n/\varepsilon^n$. In this work, we concentrate on the case of two delays and comment on the extension to the general case in Sec. V. Note that the time scales of the time delays need not satisfy $\tau_1/\tau_2 \sim \varepsilon$ in the general case. In such a case, the normal form may deviate from the Ginzburg-Landau equation, which is derived in the present section.

The characteristic equation, which determines the stability of the zero steady state $z = 0$, is obtained by linearizing Eq. (1) and substituting $z = e^{\lambda t}$:

$$\chi(\lambda, \varepsilon) := \lambda - a - be^{-\lambda/\varepsilon} - ce^{-\lambda\kappa/\varepsilon^2} = 0. \quad (5)$$

The stability of the steady state is equivalent to the fact that all roots λ of Eq. (5) have negative real parts. We assume that a, b , and c do not depend on ε .

Although the solutions to Eq. (5) are not given explicitly, their approximations can be found using the smallness of ε [12–14,33,34] (largeness of the delays),

$$\lambda = \gamma_0 + i\omega_0 + \varepsilon(\gamma_1 + i\omega_1) + \varepsilon^2(\gamma_2 + i\omega_2), \quad (6)$$

where γ_j and ω_j are real unknowns, which do not scale with ε . Depending on the leading terms in the real part of this expansion, the system may develop different types of instabilities: if $\gamma_0 > 0$, there is strong instability induced by the instantaneous term [12,13,33,35]. If $\gamma_0 = 0$ but $\gamma_1 > 0$, there is a weak instability caused by the effect of the τ_1 feedback [12–14]. In this case, the τ_2 feedback does not play an important role. Hence, in order for the second delay to play the destabilizing role, one needs $\gamma_0 = \gamma_1 = 0$ and γ_2 to become positive. Let us consider this in more detail and substitute Eq. (6) into Eq. (5). We obtain the following equation:

$$\begin{aligned} & \gamma_0 + i\omega_0 + \varepsilon(\gamma_1 + i\omega_1) + \varepsilon^2(\gamma_2 + i\omega_2) - a \\ & - be^{-(\gamma_0 + i\omega_0 + \varepsilon(\gamma_1 + i\omega_1) + \varepsilon^2(\gamma_2 + i\omega_2))/\varepsilon} \\ & - ce^{-(\gamma_0 + i\omega_0 + \varepsilon(\gamma_1 + i\omega_1) + \varepsilon^2(\gamma_2 + i\omega_2))\kappa/\varepsilon^2} = 0 \end{aligned} \quad (7)$$

for the unknowns ω_j and γ_j .

Our aim now is to derive the conditions under which the steady state is destabilized and the destabilization is on the order of the largest time delay τ_2 . We will see that these conditions are as follows: $a < 0$, $|b| < |a|$, and $P = a + |b| + |c| > 0$, with $P = 0$ playing the role of the destabilization threshold. To make the following reasoning more clear, we split it into steps.

Step 1: Identifying singular terms. Equation (7) contains terms that can become singular with $\varepsilon \rightarrow 0$:

$$be^{-(\gamma_0 + i\omega_0)/\varepsilon} - ce^{-[\gamma_0 + i\omega_0 + \varepsilon(\gamma_1 + i\omega_1)]\kappa/\varepsilon^2}.$$

While the fast oscillating phases $i\omega_0/\varepsilon$, $i\omega_0/\varepsilon^2$, and $i\omega_1/\varepsilon$ are not harmful (the amplitude is bounded), the remaining terms may become unbounded with decreasing ε . This is the case when either γ_0 or γ_1 is negative. Hence, the first solvability conditions are $\gamma_0 \geq 0$ and $\gamma_1 \geq 0$.

Step 2: Conditions for the absence of a strongly unstable spectrum. The condition $a > 0$ implies the existence of a characteristic root with strictly positive $\gamma_0 \approx a > 0$. Indeed, the solution $\lambda = a > 0$ solves the leading terms from Eq. (7) that are not vanishing with ε . All other terms become exponentially small of order $e^{-a/\varepsilon}$ and smaller. This leads to the appearance of a solution in very close proximity to $\lambda = a$ for small ε . Such a situation is called strong instability of the zero steady state; see also [13,18,33] for rigorous proof, or [35] where it is called the anomalous spectrum. As was already mentioned, we would like to avoid such a case, since the perturbations are growing here on the time interval of order $1/a \sim 1$, which is much smaller than time delays. In such a case, there is no chance to see high correlations for the times $\tau_1 = 1/\varepsilon$ or $\tau_2 = \kappa/\varepsilon^2$. Hence, we make the following assumption, which guarantees that $\gamma_0 = 0$ and there is no strongly unstable spectrum:

Assumption (I):

$$a < 0.$$

In fact, this assumption represents the stability of the system without feedbacks. Under assumption (I), one has $\gamma_0 = 0$, and the expansion (7) reduces to

$$i\omega_0 + \varepsilon\gamma_1 + \varepsilon^2\gamma_2 - a - be^{-(i\omega_0 + \varepsilon\gamma_1 + \varepsilon^2\gamma_2)/\varepsilon} - ce^{-(i\omega_0 + \varepsilon\gamma_1 + \varepsilon^2\gamma_2)\kappa/\varepsilon^2} = 0, \tag{8}$$

where the higher-order terms $\varepsilon i\omega_1 + \varepsilon^2 i\omega_2$ are omitted.

Step 3: Conditions for the absence of the τ_1 spectrum. Now let us find the conditions for which $\gamma_1 = 0$, since otherwise the perturbations will grow exponentially on the time scales of the order $1/\varepsilon\gamma_1 \sim \tau_1$, and no correlation of the time scale τ_2 can be observed. For this, we assume $\gamma_1 > 0$ (it cannot be negative according to Step 1). Then the nonvanishing terms from Eq. (8) are

$$i\omega_0 - a - be^{-(i\omega_0/\varepsilon + \gamma_1)} = 0. \tag{9}$$

From Eq. (9), one obtains

$$\gamma_1 = -\ln \left| \frac{i\omega_0 - a}{b} \right| = -\frac{1}{2} \ln \frac{\omega_0^2 + a^2}{|b|^2} \tag{10}$$

and

$$\omega_0 = -\varepsilon \arg \left[\frac{i\omega_0 - a}{b} \right] + \varepsilon 2\pi k, \quad k \in \mathbb{Z}. \tag{11}$$

Equation (11) allows for a countable set $\omega_{0,k}$ of solutions for ω_0 . It is not difficult to see that $|\omega_{0,k+1} - \omega_{0,k}| \sim \varepsilon$, i.e., for small ε they are covering densely any interval $-L < \omega_0 < L$. For any such ω_0 , the real part γ_1 is given by $\gamma_1(\omega_0)$ from (10). This part of the spectrum was called pseudocontinuous [13,18,33–35], since with $\varepsilon \rightarrow 0$ the solutions are converging to a curve $\lambda = \varepsilon\gamma_1(\omega_0) + i\omega_0$ in the complex plane, and this curve describes the stability properties.

We are interested in the case when the function γ_1 becomes negative,

$$\gamma_1(\omega_0) = -\frac{1}{2} \ln \frac{\omega_0^2 + a^2}{|b|^2} < 0 \tag{12}$$

for all ω_0 , thus contradicting our assumption $\gamma_1 > 0$. It is easy to see that (12) holds for all ω_0 if and only if $|a| > |b|$, which becomes our second assumption:

Assumption (II):

$$|a| > |b|.$$

Under assumptions (I) and (II), the simplified ansatz [instead of (6)] capturing the leading terms of the spectrum is

$$\lambda = i\omega_0 + \varepsilon^2\gamma_2 \tag{13}$$

and the expansion (7) reads

$$i\omega_0 + \varepsilon^2\gamma_2 - a - be^{-(i\omega_0 + \varepsilon^2\gamma_2)/\varepsilon} - ce^{-(i\omega_0 + \varepsilon^2\gamma_2)\kappa/\varepsilon^2} = 0. \tag{14}$$

Step 4: Expression for the τ_2 spectrum. From Eq. (14), the nonvanishing terms with $\varepsilon \rightarrow 0$ are

$$i\omega_0 - a - be^{-i\omega_0/\varepsilon} - ce^{-i\kappa\omega_0/\varepsilon^2 - \kappa\gamma_2} = 0. \tag{15}$$

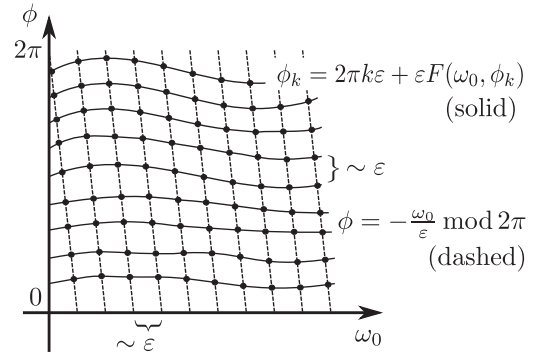


FIG. 6. Geometric representation of solutions to Eqs. (18) and (19). The solutions are given as the intersection points of two functions: $\phi = -\omega_0/\varepsilon \bmod 2\pi$ and $\phi = \phi_k(\omega_0)$, where the latter is given implicitly by Eq. (19). Since the distance between the neighboring solutions is $\sim \varepsilon$, the distance from any point of the domain to a solution is also $\sim \varepsilon$.

Equation (15) can be rewritten as

$$\frac{i\omega_0 - a - be^{-i\omega_0/\varepsilon}}{c} = e^{-i\kappa\omega_0/\varepsilon^2 - \kappa\gamma_2}. \tag{16}$$

Taking the absolute value of Eq. (16), one obtains

$$\gamma_2 = -\frac{1}{2\kappa} \ln \frac{1}{|c|^2} (|\omega_0 - |b|\sin(\phi + \phi_b)|^2 + [a + |b|\cos(\phi + \phi_b)]^2), \tag{17}$$

where $\phi_b := \arg b$ and

$$\phi = -\omega_0/\varepsilon. \tag{18}$$

By taking the phase of Eq. (16), we obtain

$$\frac{1}{\varepsilon}\phi = \arg \left(\frac{i\omega_0 - a - be^{i\phi}}{c} \right) + 2\pi k, \quad k \in \mathbb{Z}. \tag{19}$$

Step 5: Showing that solutions (ω_0, ϕ) of Eqs. (18) and (19) are covering densely a whole domain $\phi \in [0, 2\pi]$, $\omega_0 \in [-L, L]$ with some $L > 0$. Let us discuss the properties and meaning of the obtained Eqs. (17)–(19). Omitting a detailed analytical investigation of Eq. (19), we illustrate and argue geometrically that the set of solutions (ω_0, ϕ) of Eqs. (18) and (19) covers a domain $\omega_0 \in [-L, L], \phi \in [0, 2\pi]$ such that for any point (ω_0, ϕ) from this domain, there is a solution to Eqs. (18) and (19), which is $O(\varepsilon)$ close to (ω_0, ϕ) . The corresponding geometric arguments are illustrated in Fig. 6. Equation (18) determines the set of lines with the slope ε , and Eq. (19) determines the set of functions $\phi_k(\omega_0)$, which are shifted by approximately $2\pi\varepsilon$. The solutions (ω_0, ϕ) are given by the intersection points. Hence, the distance from any point in the domain to a nearby solution is of the order ε .

As a result, in the limit of large delays (small ε), we obtain the asymptotically continuous set of eigenvalues,

$$\lambda(\omega_0, \phi) = i\omega_0 + \varepsilon^2\gamma_2(\omega_0, \phi), \tag{20}$$

with γ_2 given by Eq. (17), and ω_0 and ϕ can be considered as continuous and independent parameters.

Step 6: Condition for the destabilization of the steady state by the τ_2 feedback. Finally, using the eigenvalue approximation by Eq. (20), one can obtain the stability conditions. If the condition $|c| < -a - |b|$ is satisfied, the function $\gamma_2(\omega_0, \phi)$ is negative for all ω_0 and ϕ , implying the stability of the steady state. Otherwise, γ_2 becomes positive and the steady state is unstable for all small enough ε . In this case, a nontrivial dynamics is expected.

The obtained conditions determine when the τ_2 feedback destabilizes the steady state. Namely, we have $a < 0$, $|b| < |a|$, and

$$P = a + |b| + |c|, \quad (21)$$

with P as the destabilization parameter. The desired destabilization occurs for positive values of P .

B. Derivation of the normal form

1. Equation close to the destabilization

Taking into account that the perturbation parameter is given by Eq. (21), as well as Assumptions (I) and (II), the unperturbed system ($P = 0$) can be written as

$$z'(t) = az(t) + bz(t - 1/\varepsilon) - (a + |b|)e^{i\phi_c} z(t - \kappa/\varepsilon^2) + dz(t)|z(t)|^2, \quad (22)$$

where we substituted $c = (-a - |b|)e^{i\phi_c}$ in order to fulfill Eq. (21) with $P = 0$. We also substituted $\tau_1 = 1/\varepsilon$ and $\tau_2 = \kappa/\varepsilon^2$. According to assumptions (I) and (II), we have also $a < 0$ and $|b| < -a$. Furthermore, we consider the

$$\begin{aligned} z\left(t - \frac{1}{\varepsilon}\right) &= \varepsilon u_1(T_1 - 1, \dots) + \varepsilon^2[-D_2 u_1(T_1 - 1, \dots) + u_2(T_1 - 1, \dots)] \\ &\quad + \varepsilon^3\left[-D_3 u_1(T_1 - 1, \dots) + \frac{1}{2}D_2^2 u_1(T_1 - 1, \dots) - D_2 u_2(T_1 - 1, \dots) + u_3(T_1 - 1, \dots)\right], \\ z\left(t - \frac{\kappa}{\varepsilon^2}\right) &= \varepsilon u_1\left(T_1 - \frac{\kappa}{\varepsilon}, T_2 - \kappa, \dots\right) + \varepsilon^2\left[-D_3 u_1\left(T_1 - \frac{\kappa}{\varepsilon}, T_2 - \kappa, \dots\right) + u_2\left(T_1 - \frac{\kappa}{\varepsilon}, T_2 - \kappa, \dots\right)\right] \\ &\quad + \varepsilon^3\left[\frac{1}{2}D_{33}^2 u_1\left(T_1 - \frac{\kappa}{\varepsilon}, T_2 - \kappa, \dots\right) - D_4 u_1\left(T_1 - \frac{\kappa}{\varepsilon}, T_2 - \kappa, \dots\right) - D_3 u_2\left(T_1 - \frac{\kappa}{\varepsilon}, T_2 - \kappa, \dots\right)\right. \\ &\quad \left.+ u_3\left(T_1 - \frac{\kappa}{\varepsilon}, T_2 - \kappa, \dots\right)\right], \end{aligned}$$

and the nonlinear terms start from the third order in ε :

$$z(t)|z(t)|^2 = \varepsilon^3 u_1 |u_1|^2 + \dots$$

In the following, we consider separately terms of different orders in ε .

3. Solvability conditions for the order- ε terms

By substituting the obtained expansions into Eq. (23), and leaving only the terms of the lowest order ε , we obtain

$$\begin{aligned} au_1(T_1, T_2, \dots) + bu_1(T_1 - 1, T_2, \dots) \\ = (a + |b|)e^{i\phi_c} u_1(T_1 - \kappa/\varepsilon, T_2 - \kappa, \dots). \end{aligned} \quad (25)$$

perturbed system

$$z'(t) = (a + p\varepsilon^2)z(t) + bz(t - 1/\varepsilon) - (a + |b|)e^{i\phi_c} z(t - 1/\varepsilon^2) + dz(t)|z(t)|^2, \quad (23)$$

where $P = p\varepsilon^2$ is a small perturbation parameter. It should be pointed out that the choice of the parameter that is perturbed (here it is a) is arbitrary. One can consider also more general perturbations of the other parameters b, c , as well as a nonlinearity. As soon as the smallness of the perturbation is ε^2 , the following derivation of the normal form remains practically the same. The reason for the ε^2 order of the perturbation is the same as in the case of the normal form for the Hopf bifurcation [36].

2. Multiscale ansatz

We use the following general multiscale ansatz:

$$z(t) = \sum_{j=1} \varepsilon^j u_j(T_1, T_2, T_3, T_4, \dots), \quad (24)$$

where $T_k = \varepsilon^k t$ are different time scales, and the unknown functions u_j are bounded. The factor ε in front indicates that we are interested in small solutions close to the destabilization.

The main idea is to substitute the ansatz (24) into the dynamical equation (23) and split terms with different smallness with respect to ε . Before doing this, let us calculate different terms. The time derivative is

$$z'(t) = \varepsilon^2 D_1 u_1 + \varepsilon^3 (D_2 u_1 + D_1 u_2) + \dots,$$

where D_k are corresponding partial derivatives $\partial/\partial T_k$. The first and the second delayed terms up to the order ε^3 read

Equation (25) can be considered as a linear discrete dynamical system (two-dimensional map) of two variables (T_1, T_2) , which determines the value of the function u_1 in the point (T_1, T_2) given the values of that function in the points $(T_1 - 1, T_2)$ and $(T_1 - \kappa/\varepsilon, T_2 - \kappa)$. The only possible bounded solutions in such a system, due to the linearity, are solutions satisfying $u_1(T_1, T_2, \dots) = e^{i\psi_1} u_1(T_1 - 1, T_2, \dots)$ and $u_1(T_1, T_2, \dots) = e^{i\psi_2} u_1(T_1 - \kappa/\varepsilon, T_2 - \kappa, \dots)$ with some phases ψ_1 and ψ_2 . By substituting it into Eq. (25), we obtain

$$a + |b|e^{-i\psi_1 + i\phi_c} = (a + |b|)e^{i\phi_c - i\psi_2}. \quad (26)$$

Since $a < 0$ and $|b| < a$ by assumptions (I) and (II), Eq. (26) is only solvable when the corresponding arguments are zero, thus

$\psi_1 = \phi_b$ and $\psi_2 = \phi_c$. Therefore, we arrive at the conditions

$$u_1(T_1, T_2) = e^{i\phi_b} u_1(T_1 - 1, T_2), \quad (27)$$

$$\begin{aligned} u_1(T_1, T_2) &= e^{i\phi_c} u_1\left(T_1 - \frac{\kappa}{\varepsilon}, T_2 - \kappa\right) \\ &= e^{i(\phi_c - \phi_b[\kappa/\varepsilon])} u_1\left(T_1 - \left\{\frac{\kappa}{\varepsilon}\right\}_f, T_2 - \kappa\right). \end{aligned} \quad (28)$$

Here $\{\cdot\}_f$ is the fractional and $[\cdot]$ is the integer parts of a number. Note that $\kappa/\varepsilon = \tau_2/\tau_1$. In the case when the ratio of the delay times is integer $\{\frac{\kappa}{\varepsilon}\}_f = 0$, the condition (28) can be simplified as

$$u_1(T_1, T_2) = e^{i(\phi_c - \phi_b[\kappa/\varepsilon])} u_1(T_1, T_2 - \kappa).$$

Equations (27) and (28) are the solvability conditions resulting from the terms proportional to ε . In fact, they will lead to boundary conditions for the resulting normal form equation. From another perspective, the discrete dynamical system (25) obtained to this order is equivalent to the limiting discrete map obtained by setting the derivative to zero. Such a limiting map is often used in the case of one large delay [1,37] for an approximate description of the dynamics of a delay system. In our case, such a limiting map is neutrally stable for the unperturbed system (22).

4. Solvability conditions for the order ε^2

By collecting terms of the order ε^2 , we obtain

$$\begin{aligned} D_1 u_1 &= -b D_2 u_1(T_1 - 1, T_2) \\ &+ (a + |b|) e^{i\phi_c} D_3 u_1\left(T_1 - \frac{\kappa}{\varepsilon}, T_2 - \kappa\right) + a u_2 \\ &+ b u_2(T_1 - 1, T_2) \\ &- [a + |b|] e^{i\phi_c} u_2\left(T_1 - \frac{\kappa}{\varepsilon}, T_2 - \kappa\right). \end{aligned}$$

The parts of the obtained equation with the terms u_2 have the same form as Eq. (25). By collecting the terms with u_2 , one can see that u_2 satisfies the same solvability conditions (27) and (28) as u_1 . The remaining terms are

$$\begin{aligned} D_1 u_1 &= -b D_2 u_1(T_1 - 1, T_2) \\ &+ (a + |b|) e^{i\phi_c} D_3 u_1\left(T_1 - \frac{\kappa}{\varepsilon}, T_2 - \kappa\right). \end{aligned}$$

We remind the reader here that the arguments T_3, T_4, \dots are omitted for brevity. Taking into account the conditions (27) and (28), one can eliminate the terms with shifted arguments and obtain

$$D_1 u_1 = -|b| D_2 u_1 + (a + |b|) D_3 u_1. \quad (29)$$

The obtained Eq. (29) connects the derivatives $D_1 u_1, D_2 u_1$, and $D_3 u_1$, i.e., a transport equation. Solutions of Eq. (29) are arbitrary functions of the form (solutions along characteristics)

$$u_1(T_1, T_2, T_3, T_4) = \Phi(T_4, T_1 - \nu T_3, T_2 - \nu|b|T_3), \quad (30)$$

where we denoted $\nu := (-a - |b|)^{-1} > 0$. The new arguments are

$$x = T_1 - \nu T_3, \quad y = T_2 - \nu|b|T_3, \quad \theta = T_4. \quad (31)$$

We do not write here the slower variables T_5, T_6, \dots , since the dynamics in which we are interested are limited to T_4 . A summary of the solvability conditions from the ε^2 terms is given by Eq. (30). This relation tells us that there is a simple transport on the time scale $\varepsilon^3 t$, which results in the relation (30) between the time scales. As we will see later, this transport will be responsible for the drift in the spatiotemporal representation of the solutions of the delay system; see Sec. III C.

It is remarkable that both the drift and the boundary conditions are determined by the linear terms only. This is due in particular to the cubic nonlinearity of our system. This remains true also for higher-order nonlinearities.

5. Solvability conditions for the order ε^3

The final order, which we consider here, is ε^3 , and it will lead to the normal form equation of the Ginzburg-Landau type for the function $\Phi(\theta, x, y)$ introduced above by Eqs. (30) and (31). By collecting terms of the order ε^3 , we obtain

$$\begin{aligned} D_2 u_1 + D_1 u_2 &= a u_3 + p u_1 + b \left\{ \frac{1}{2} D_{22} u_1(T_1 - 1) \right. \\ &- D_3 u_1(T_1 - 1) - D_2 u_2(T_1 - 1) \\ &+ u_3(T_1 - 1) \left. \right\} + d u_1 |u_1|^2 \\ &- (a + |b|) e^{i\phi_c} \left\{ \frac{1}{2} D_{33} u_1\left(T_1 - \frac{\kappa}{\varepsilon}, T_2 - \kappa\right) \right. \\ &- D_4 u_1\left(T_1 - \frac{\kappa}{\varepsilon}, T_2 - \kappa\right) \\ &- D_3 u_2\left(T_1 - \frac{\kappa}{\varepsilon}, T_2 - \kappa\right) \\ &+ u_3\left(T_1 - \frac{\kappa}{\varepsilon}, T_2 - \kappa\right) \left. \right\}. \end{aligned}$$

The terms with u_3 can be eliminated assuming the same conditions (25) as for u_1 and u_2 . Further, the u_2 terms satisfy the transport equation (29). The remaining part contains only terms with u_1 . It can be simplified using (27) and (28) by eliminating shifted arguments, leading to the expression

$$\begin{aligned} -(a + |b|) D_4 u_1 &= p u_1 - D_2 u_1 - |b| D_3 u_1 + \frac{|b|}{2} D_{22} u_1 \\ &- (a + |b|) \frac{1}{2} D_{33} u_1 + d u_1 |u_1|^2. \end{aligned} \quad (32)$$

Now we use the properties given by Eqs. (30) and (31) and rewrite Eq. (32) with respect to the function Φ and new coordinates x, y , and θ :

$$\begin{aligned} \nu^{-1} \Phi_\theta &= p \Phi + \nu|b| \Phi_x - (1 - \nu|b|^2) \Phi_y \\ &+ \frac{\nu}{2} (\Phi_{xx} + 2|b| \Phi_{xy} + |ab| \Phi_{yy}) + d \Phi |\Phi|^2. \end{aligned} \quad (33)$$

The obtained equation (33) is already the Ginzburg-Landau-type normal form equation, at which we are aiming. The

corresponding boundary conditions follow from the ε^1 solvability conditions (27) and (28), which should be rewritten with respect to Φ and have the following form:

$$\Phi(x, y, \theta) = e^{i\phi_b} \Phi(x - 1, y, \theta), \quad (34)$$

$$\Phi(x, y, \theta) = e^{i(\phi_c - \phi_b \lfloor \frac{x}{\varepsilon} \rfloor)} \Phi\left(x - \left\{\frac{\kappa}{\varepsilon}\right\}_f, y - \kappa, \theta\right). \quad (35)$$

In the case when the ration τ_2/τ_1 is integer, and, hence $\{\frac{\kappa}{\varepsilon}\}_f = 0$, the second condition (35) reduces to

$$\Phi(x, y, \theta) = e^{i(\phi_c - \phi_b \tau_2/\tau_1)} \Phi(x, y - \kappa, \theta).$$

6. Summary of the normal form equations

Summarizing, we have obtained the normal form equation (33), which should be equipped with the boundary conditions (34) and (35). The equation is a Ginzburg-Landau-type system. The solutions Φ of this equation are supposed to approximate the solutions of the delayed equation (23), with the following relation between the solutions:

$$z(t) = \varepsilon \Phi(\varepsilon^4 t, \varepsilon t - \nu \varepsilon^3 t, \varepsilon^2 t - \nu |b| \varepsilon^3 t) + \dots \quad (36)$$

The relation (36) follows directly from Eqs. (24) and (30). Note that the temporal variable $\theta = \varepsilon^4 t$ of the function Φ is the slowest time scale. This means that the typical Ginzburg-Landau dynamics given by the temporal changes according to the dynamical Eq. (33) will be visible on the time scales $\sim \tau^4 = 1/\varepsilon^4$ in the dynamics of the delay systems. We will call the variable θ *pseudotime*. The two other variables x and y are scales $T_1 = \varepsilon t$ and $T_2 = \varepsilon^2 t$ corrected by a shift on the time scale $T_3 = \varepsilon^3 t$. We will call these variables *pseudospace*. The first pseudospacial variable is connected to the first time delay τ_1 , since the change of the real time t by an amount τ_1 corresponds to the change of x by 1. Similarly, the second pseudospacial variable y is connected to τ_2 .

Let us describe how the STR in Figs. 3 and 4 have been obtained. The spatial coordinates in the figures are as introduced above:

$$x = (1 - \nu \varepsilon^2) \varepsilon t, \quad y = (1 - \nu |b| \varepsilon) \varepsilon^2 t. \quad (37)$$

By this relation, for any time point t , there is the corresponding point (x, y) in the pseudospace and the point of the pseudotime θ , and the value of the function Φ in this point is given by $\Phi(\theta, x, y) := z(t)/\varepsilon$. In this way, given a solution $z(t)$ of the delayed equation (1), one finds the value of the function Φ on some points in the space $(x(t), y(t), \theta(t))$ determined by (31). If ε is small, then these points are densely located with distances of the order ε , and a good approximation of the spatiotemporal function Φ can be made. The resulting functions are plotted in Figs. 3 and 4 as a color plot for some fixed value of the pseudotime θ . As the pseudotime is varied, one obtains dynamical patterns; see the supplemental material to Ref. [29] for additional details.

7. Discussion of boundary conditions

The obtained boundary condition (35) still depends on the parameter ε , although in a nonsingular way:

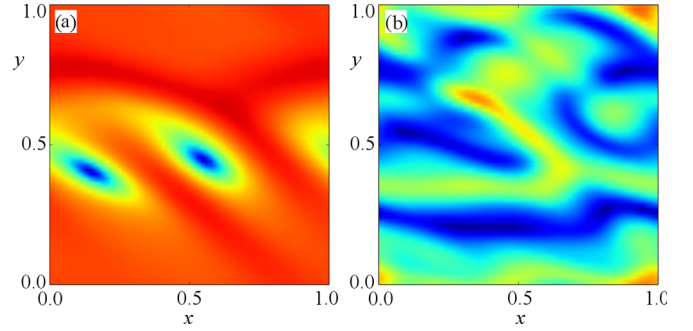


FIG. 7. (Color online) Snapshots for the solutions of the normal form equation (38). (a) Spiral defects, parameter values: $p = 250$, $a_1 = 1.11$, $a_2 = -1.22$, $a_3 = 1.39$, $a_4 = 1.11$, $a_5 = 0.56$, and $d = -0.75 + i$. (b) Defect turbulence, parameter values are the same except for $d = -0.1 + i$. Initial values are random and close to zero.

(i) The simplest case of the periodic boundary conditions on the domain $G_1 = [0, 1] \times [0, \kappa]$ arises for $\phi_b = \phi_c = 0$ (real positive parameters c and b) and $\tau_2/\tau_1 = j$, where j is an integer number.

(ii) If only the assumption $\tau_2/\tau_1 = j$ is made, then the boundary condition makes just a phase shift on the boundaries of the domain G_1 .

(iii) If no assumptions are made, the condition (35) connects not only the points on the boundary of the domain, but also a point inside $(x = x - \{\kappa/\varepsilon\}_f, y = y - \kappa)$. In this case, it is reasonable to consider classes of systems corresponding to the same value of $\{\kappa/\varepsilon\}_f = \mu < 1$. Any sequence ε_j of the form $\varepsilon_j = \kappa/(\mu + j)$, $j = 1, 2, \dots$, corresponds to the same class of systems, which involves the points $(x = x - \mu, y = y - \kappa)$ as a boundary condition.

8. Reduced normal form by neglecting boundary conditions

In many cases, the main features of the dynamics are independent from the boundary conditions (“bulk” dynamics), similar to the attainment of the thermodynamic limit in a spatially extended system (see, e.g., [38]). By neglecting boundary conditions, one can eliminate the convective terms with Φ_x and Φ_y and cross-derivative Φ_{xy} in the normal form (33) by using an appropriate coordinate transformation. The resulting equation has a simpler form:

$$\Phi_\theta = p\Phi + |a|^{-1}(\Phi_{xx} + \Phi_{yy}) + d\Phi|\Phi|^2, \quad (38)$$

with the real diffusion coefficient $|a|^{-1}$. The dynamics of (38) is known [38–40] to possess various phase transitions, spiral defects (e.g., for $d = -0.75 + i$), and defect turbulence (e.g., for $d = -0.1 + i$).

We found numerically a good qualitative correspondence between the dynamics of systems (38) and (1) [29]. As an example, we report in Figs. 7(a) and 7(b) the results of the integration of (38) in the cases corresponding to Figs. 3 and 4, respectively.

C. Drift

1. Drift in multiscale temporal dynamics

The dynamics of patterns takes place on the slow time scale ε^{-4} , as follows from (36) and (33). By restricting the

consideration up to time scales ε^{-3} , one observes just a drift. In order to see this, let us introduce the uncorrected, “natural,” spatial variables $\bar{x} = \varepsilon t$, $\bar{y} = \varepsilon^2 t$, and $\bar{u} = \varepsilon^3 t$ capturing the dynamics up to the scale ε^{-3} . On time scales ε^{-3} , the dynamics is described by a two-dimensional function $\Phi(\theta_0, x, y)$ with a fixed θ_0 . Taking into account the relation (31), we have $x = \bar{x} - \delta\bar{u}$ and $y = \bar{y} - |b|\delta\bar{u}$, and, hence, the solution is described by (36) with $\Phi(\theta_0, \bar{x} - \delta\bar{u}, \bar{y} - |b|\delta\bar{u})$, meaning just a translation in the natural coordinates \bar{x}, \bar{y} along the vector $\mathbf{V}_d = (-1, -|b|)$. In practical terms, this means that the dynamics in the natural coordinates \bar{x}, \bar{y} exhibit a drift on the time scale ε^{-3} , which is faster than the time scale ε^{-4} of the dynamics given by the normal form. The corrected coordinates x and y eliminate this fast drift so that the remaining variables are governed by the Ginzburg-Landau equation.

2. Drift and comoving Lyapunov exponents

The above-mentioned drift could be determined as a consequence of the properties of the maximal comoving Lyapunov exponent [41]. We give some details of its calculation, since it could be employed for a higher number of delays as well. The linearization of (1) in $z = 0$ is

$$\dot{z} = az + bz_{\tau_1} + cz_{\tau_2}. \quad (39)$$

We consider now the STR,

$$t = \sigma + n\tau_1 + m\tau_2,$$

where $\sigma \in [0, \tau_1)$, and m and n are positive integers such that $n = 0, 1, \dots, [\tau_2/\tau_1]$. The new coordinates are related to the previously introduced coordinates \bar{x}, \bar{y} , and \bar{z} , such that $\sigma \sim \bar{x}/\varepsilon$, $n \sim \bar{y}/\varepsilon$, and $m \sim \bar{z}/\varepsilon$. The multiple-scale ansatz in this case reads $z(t) = X_{n,m}(\sigma)$, and Eq. (39) is rewritten as

$$LX_{n+1,m+1}(\sigma) = bX_{n,m+1}(\sigma) + cX_{n+1,m}(\sigma), \quad (40)$$

where L is the linear operator $L = \partial_\sigma - a$. Equation (40) can be solved, e.g., using the Laplace transform, with the initial conditions $X_{n,m}^{(0)}(\sigma) = \delta_{n,1} \times \delta_{1,m} \times \delta(\sigma)$. It is found that

$$X_{n+1,m+1}(\sigma) = \left(\frac{b^n}{n!}\sigma^n\right)\left(\frac{c^m}{m!}\sigma^m\right)(b+c)e^{a\sigma}. \quad (41)$$

This expression generalizes Eq. (8) of [16].

To evaluate the maximal comoving Lyapunov exponent, we introduce the spherical coordinates $m = \rho \cos \alpha$, $n = \rho \sin \alpha \cos \beta$, $\sigma = \rho \sin \alpha \sin \beta$, and define as usual the maximal comoving Lyapunov exponent as

$$\Lambda(\alpha, \beta) = \lim_{\rho \rightarrow \infty} \frac{\log |X_{n,m}(\sigma)|}{\rho}. \quad (42)$$

Using the Stirling approximation, and after some calculations, it is found that

$$\Lambda(\alpha, \beta) = a \sin \alpha \sin \beta + [1 + \log(|b| \tan \beta)] \times \sin \alpha \cos \beta + [1 + \log(|c| \sin \beta \tan \alpha)] \times \cos \alpha. \quad (43)$$

A geometrical interpretation [see Fig. 8(a)] can be introduced using the velocity $\mathbf{V} = (\sin \beta \tan \alpha, \cos \beta \tan \alpha)$, along which the perturbations evolve with a multiplier $e^{\Lambda(\alpha, \beta)}$. The propagation cone’s boundaries can be defined as the set (α, β) such that $\Lambda(\alpha, \beta) = 0$. The bifurcation point, attained

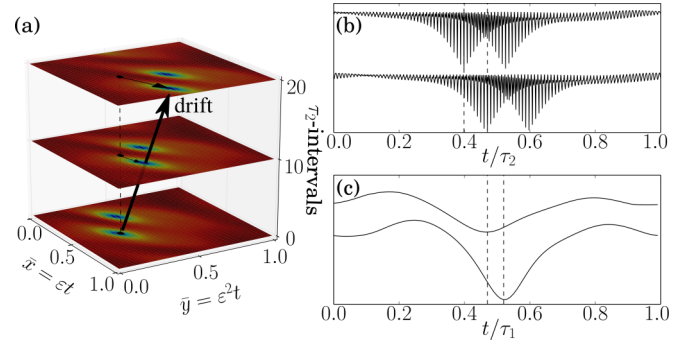


FIG. 8. (Color online) Drift in the propagation of defect structures, from the integration of (1). Parameters are those used in Fig. 1. Using the STR with the uncorrected pseudospace variables, the defects are moving in pseudotime (a). The components of the (vectorial) drift can be evidenced by plotting two successive τ_2 -long (b) and τ_1 -long slices (c). The separations between the two vertical dashed lines are \bar{y} (b) and \bar{x} (c) drift components, respectively.

when the maximum of Λ is equal to zero, is obtained at $\mathbf{V} = \mathbf{V}_0 = \left(\frac{-1}{a+|b|}, \frac{-|b|}{a+|b|}\right) = \delta\mathbf{V}_d$, corresponding to $(\alpha_0, \beta_0) = (\tan^{-1}\left(\frac{\sqrt{1+|b|^2}}{a+|b|}\right), \tan^{-1}\left(\frac{1}{|b|}\right))$. Here $\delta\mathbf{V}_d$ is the same drift obtained from the multiscale ansatz in the previous Sec. III C 1.

The components of the vectorial drift can be shown in their effects in shifting the time series at the corresponding scales; we plot in Figs. 8(b) and 8(c) such quantities along the uncorrected \bar{y} and \bar{x} variables, respectively.

The above result (43) extends the standard linear stability analysis by indicating the direction along which the destabilization takes place. We remark that, since for a choice of arbitrary parameters the angles are generically nonzero and bounded below $\pi/2$, the disturbances always propagate with a drift. We notice how the comoving exponent diverges logarithmically close to the axis $\alpha = 0$ and $\beta = 0$, i.e., instantaneous propagations are forbidden. In the opposite limit, $\alpha \rightarrow \pi/2$ ($\beta \rightarrow \pi/2$), Λ approaches the value for the single delay case $c = 0$ ($b = 0$). Finally, when both $\alpha, \beta \rightarrow \pi/2$ (infinite velocity), $\Lambda = a$ and the dynamics is governed by the local term, as expected.

IV. FROM SMALL TO LARGE DELAYS

For large delays, the normal form (33) seems to reproduce the dynamics of the delayed system (1). However, for smaller delays, differences between the two models appear and become more and more relevant. The effects, related to the finiteness of the delays involved, are similar to the (finite)-size effects observed in spatially extended systems. We can estimate those effects by evaluating the convergence of behaviors and/or statistical and dynamical indicators when decreasing the delay values. A transition is expected, where the finite-size results are significantly different (or scale differently) from the asymptotic values (or behaviors).

We report in Fig. 9 the dynamics of Eq. (1) for increasing values of $\tau_1 = \varepsilon^{-1}$ and keeping $\tau_2 = \varepsilon^{-2} = \tau_1^2$. In the left part, we show the time series obtained after a transient. The amplitude is rescaled and the time is expressed in units of τ_2 to compare the results. For the parameters used, the

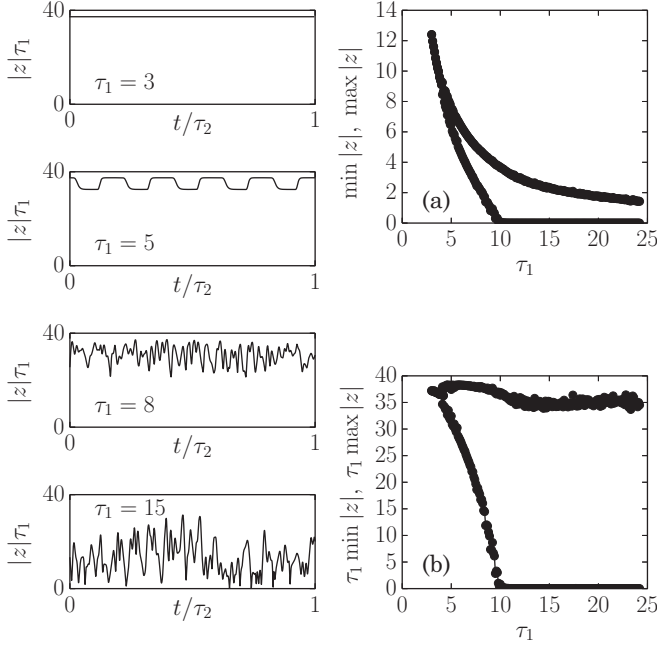


FIG. 9. Temporal series from system (1) for different values of the delays. The parameters used are those of Fig. 2. Left column: time series of $|z|$ with amplitude rescaled by τ_1 , for increasing values of τ_1 (from top to bottom: $\tau_1 = 3, 5, 8$, and 15). Time is expressed in units of τ_2 . Right: maximum and minimum of the amplitude $|z|$ (a) and of the rescaled amplitude $|z|/\varepsilon = |z|\tau_1$ (b), evaluated after a transient.

corresponding normal form displays defects turbulence, as shown in Fig. 7(b). In the delayed system, for $\tau_1 \gtrsim 15$, time series similar to those of the CGL and defects appear. For smaller values of τ_1 , the solutions converge to periodic or bounded nonzero oscillations after a transient.

This behavior is better evidenced in the right part of Fig. 9, where we plot the maximum and minimum of the amplitude (evaluated on a long interval after a transient) (a) and their rescaled values (b) as a function of τ_1 . A transition between two regimes is clearly visible at $\tau_1 \simeq 10$ ($\varepsilon \simeq 0.1$), above which a stationary defects turbulence behavior can be observed.

A more quantitative investigation is presented in Fig. 10, where we plot the contour lines of the normalized autocor-

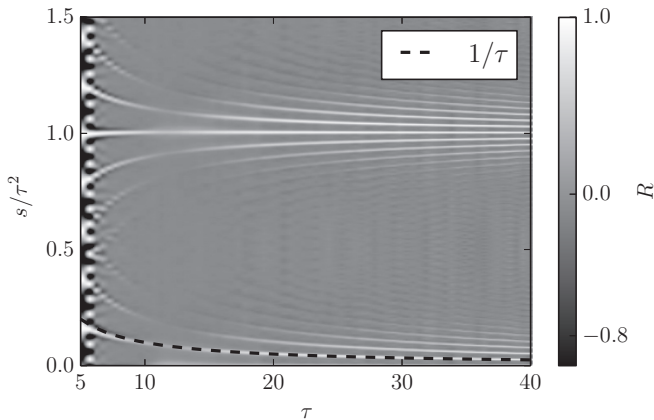


FIG. 10. Autocorrelation function R for $|z(t)|$. Dependence of the autocorrelation on the delay τ .

relation R function of the signal $|z(t)|$ as a function of τ_1 . The shift variable s is rescaled to τ_2 . As shown in the figure, the autocorrelation converges to a well-defined structure for high values of τ_1 (larger than 15), characterized by main peaks at (almost) integer values, with satellite peaks separated by $1/\tau_1$. Such structure changes for small values of τ_1 , where the satellite peaks are modulated or disappear, indicating that the dynamical regime there is drastically different.

As a further criterium, a statistical description has been introduced in Ref. [29]. In that work, the characterization of the regimes is based on the analysis of the scaling of the amplitude distribution.

From the above analysis, it is evident that finite-size (delays) effects in our system are increasingly important, leading to significant differences with the asymptotical results for $\varepsilon \geq 0.1$. While this result is specific to the case considered, we expect that a similar result can be obtained for different models in the very same way it holds for spatially extended systems.

V. HIGHER NUMBER OF DELAYS

The above considerations can be applied to an arbitrary number of delays. In the general case, we consider a dynamical system characterized by a natural time scale t_0 in the absence of feedback, with N feedback loops each with a delay τ_k ($k = 1, \dots, N$). We assume a hierarchy of magnitudes, introducing a smallness parameter $\varepsilon = t_0/\tau_1 \ll 1$ and considering $\tau_k = t_0 \varepsilon^{-k}$. The multiple scales are then defined as $T_l = \varepsilon^l t$, l being a natural number.

In this case, we expect that $\{T_l, l = 1, \dots, N\}$ are the “spatial” scales. The T_{N+1} is the scale of the “drift”; it can be measured by means, e.g., of the comoving Lyapunov exponent (on the microscopic amplitude scales) or the autocorrelation (on the macroscopic scale) method [42]. Finally, the scale for the equivalent CGL dynamics is T_{N+2} .

In the general case, we consider the STR [Eq. (3)], where the variables σ_0 , $\{n\}$, and Θ are defined by

$$\begin{aligned} [t/\tau_N] &= \Theta, \\ [(t - \Theta\tau_N)/\tau_{N-1}] &= n_{N-1}, \\ [(t - \Theta\tau_N - n_{N-1}\tau_{N-1})/\tau_{N-2}] &= n_{N-2}, \\ &\dots \\ [(t - \Theta\tau_N - n_{N-1}\tau_{N-1} - \dots - n_2\tau_2)/\tau_1] &= n_1, \\ t - \Theta\tau_N - n_{N-1}\tau_{N-1} - \dots - n_1\tau_1 &= \sigma_0. \end{aligned}$$

It is apparent that $\sigma_0 \in [0, \tau_1]$. Since the pseudospacial variables n_k can be large and are bounded by $[\tau_{k+1}/\tau_k]$, we define the rescaled pseudospacial variables $S_0 = \sigma_0/(\tau_1/t_0)$ and $S_k = n_k/(\tau_{k+1}/\tau_k)$, $k = 1, \dots, N-1$, which are confined to the interval $[0, 1]$, and the pseudotemporal variable $T = \Theta/(t/\tau_N)$. Then we have

$$\begin{aligned} \sigma_0/t_0 &= \sigma_0/\tau_1 \tau_1/t_0 = S_0 \varepsilon^{-1}, \\ n_1 \tau_1/t_0 &= n_1/(\tau_2/\tau_1)(\tau_2/\tau_1)(\tau_1/t_0) = S_1 \varepsilon^{-2}, \\ &\dots \\ n_{N-1} \tau_{N-1}/t_0 &= n_{N-1}/(\tau_N/\tau_{N-1}) \dots (\tau_1/t_0) = S_{N-1} \varepsilon^{-N}, \\ \Theta \tau_N/t_0 &= \Theta/(t/\tau_N)(t/t_0) = T \varepsilon^{-(N+1)}. \end{aligned}$$

The STR hence is rewritten as

$$\bar{t} = t/t_0 = S_0\varepsilon^{-1} + S_1\varepsilon^{-2} + \dots + S_{N-1}\varepsilon^{-N} + T\varepsilon^{-(N+1)}. \quad (44)$$

The STR can now be related to the multiscale analysis: the dynamics on the time scale $T_l = \varepsilon^l t$ is visible on the coordinate l only, since the scales $k < l$ are too fast and the $k > l$ too slow.

The drift (over the scale T_{N+1}) and the effective CGL dynamics (in the comoving reference frame, with scales equal to or longer than T_{N+2}) can be visualized in the STR using a time interval $t/\tau_N \simeq \varepsilon^{-1}$ and $t/\tau_N \simeq \varepsilon^{-2}$, respectively.

The above definitions set the formal framework for a discussion in a general case and provide an interpretation of the STR; however, the rigorous derivation of the normal forms or even the interpretation of the interplay between the different time scales will have to be discussed case by case.

VI. CONCLUSIONS

We have presented a class of dynamical systems, namely multiple, hierarchically long-delayed systems. In the case of two delays, we have shown that the complex time series obtained via the numerical integration of a Stuart-Landau oscillator with two feedbacks are encoding, in a suitable representation, the evolution of two-dimensional spatial patterns. The equivalent space and temporal coordinates are related to specific time scales of the system, thus suggesting the

possibility of a multiscale approach. Accordingly, we derived a Ginzburg-Landau normal form close to the bifurcation point: such a model, in the limit of infinite size (long delays), reproduces the observed behaviors of the delay system. The approach allows for a clear definition of the spacelike and timelike variables in terms of the time scales of the original system. The definition of a drift and the identification of the (pseudo) time scale where it can be observed and its properties in terms of the maximum comoving Lyapunov exponent are also given. Moreover, we discussed the limit of the correspondence set by finite-size effects by evaluating different qualitative and quantitative indicators. Finally, a formal framework in the general case of n delays has been introduced and suggested as the starting point for the analysis of different models and/or experimental setups.

ACKNOWLEDGMENTS

We acknowledge the DFG for financial support in the framework of International Research Training Group 1740, the European Research Council (ERC-2010-AdG 267802, Analysis of Multiscale Systems Driven by Functionals), and useful discussions with A. Politi. The work has been partially carried out during the visit of S. Yanchuk at ISC in the framework of the STM–Short Term Mobility program, financed by CNR.

-
- [1] T. Erneux, *Applied Delay Differential Equations, Vol. 3 of Surveys and Tutorials in the Applied Mathematical Sciences* (Springer, New York, 2009).
- [2] X. Li, A. B. Cohen, T. E. Murphy, and R. Roy, *Opt. Lett.* **36**, 1020 (2011).
- [3] J. Zamora-Munt, C. Masoller, J. Garcia-Ojalvo, and R. Roy, *Phys. Rev. Lett.* **105**, 264101 (2010).
- [4] G. Giacomelli, F. Marino, M. A. Zaks, and S. Yanchuk, *Europhys. Lett.* **99**, 58005 (2012).
- [5] M. C. Soriano, J. Garcia-Ojalvo, C. R. Mirasso, and I. Fischer, *Rev. Mod. Phys.* **85**, 421 (2013).
- [6] R. Szalai and G. Orosz, *Phys. Rev. E* **88**, 040902 (2013).
- [7] E. M. Izhikevich, *Neural Computat.* **18**, 245 (2006).
- [8] L. Appeltant, M. C. Soriano, G. Van der Sande, J. Danckaert, S. Massar, J. Dambre, B. Schrauwen, C. R. Mirasso, and I. Fischer, *Nat. Commun.* **2**, 468 (2011).
- [9] J. K. Hale and S. M. V. Lunel, *Introduction to Functional Differential Equations* (Springer-Verlag, New York, 1993).
- [10] J. D. Farmer, *Physica D* **4**, 366 (1982).
- [11] G. Giacomelli, S. Lepri, and A. Politi, *Phys. Rev. E* **51**, 3939 (1995).
- [12] S. Heiligenthal, T. Dahms, S. Yanchuk, T. Jüngling, V. Flunkert, I. Kanter, E. Schöll, and W. Kinzel, *Phys. Rev. Lett.* **107**, 234102 (2011).
- [13] M. Lichtner, M. Wolfrum, and S. Yanchuk, *SIAM J. Math. Anal.* **43**, 788 (2011).
- [14] O. D’Huys, S. Zeeb, T. Jüngling, S. Heiligenthal, S. Yanchuk, and W. Kinzel, *Europhys. Lett.* **103**, 10013 (2013).
- [15] J. Sieber, M. Wolfrum, M. Lichtner, and S. Yanchuk, *Discrete Contin. Dyn. Syst. A* **33**, 3109 (2013).
- [16] G. Giacomelli and A. Politi, *Phys. Rev. Lett.* **76**, 2686 (1996).
- [17] M. Nizette, *Physica D* **183**, 220 (2003).
- [18] M. Wolfrum and S. Yanchuk, *Phys. Rev. Lett.* **96**, 220201 (2006).
- [19] G. Giacomelli, F. Marino, M. A. Zaks, and S. Yanchuk, *Phys. Rev. E* **88**, 062920 (2013).
- [20] F. T. Arecchi, G. Giacomelli, A. Lapucci, and R. Meucci, *Phys. Rev. A* **45**, R4225 (1992).
- [21] T. Hikihara and Y. Ueda, *Chaos* **9**, 887 (1999).
- [22] M. Bestehorn, E. V. Grigorieva, H. Haken, and S. A. Kaschenko, *Physica D* **145**, 110 (2000).
- [23] A. L. Franz, R. Roy, L. B. Shaw, and I. B. Schwartz, *Phys. Rev. E* **78**, 016208 (2008).
- [24] S. Yanchuk, L. Lücken, M. Wolfrum, and A. Mielke, *Discrete Contin. Dyn. Syst. A* **35**, 537 (2015).
- [25] B. Garbin, J. Javaloyes, G. Tissoni, and S. Barland, *Nat. Commun.* **6**, 5915 (2015).
- [26] G. Giacomelli, R. Meucci, A. Politi, and F. T. Arecchi, *Phys. Rev. Lett.* **73**, 1099 (1994).
- [27] C. Masoller, *Chaos* **7**, 455 (1997).
- [28] L. Larger, B. Penkovsky, and Y. Maistrenko, *Phys. Rev. Lett.* **111**, 054103 (2013).
- [29] S. Yanchuk and G. Giacomelli, *Phys. Rev. Lett.* **112**, 174103 (2014).
- [30] G. Giacomelli and A. Politi, *Physica D* **117**, 26 (1998).
- [31] X. Porte, O. D’Huys, T. Jüngling, D. Brunner, M. C. Soriano, and I. Fischer, *Phys. Rev. E* **90**, 052911 (2014).
- [32] G. Giacomelli, F. Marin, and M. Romanelli, *Phys. Rev. A* **67**, 053809 (2003).
- [33] S. Yanchuk and M. Wolfrum, *SIAM J. Appl. Dyn. Syst.* **9**, 519 (2010).
- [34] M. Wolfrum, S. Yanchuk, P. Hövel, and E. Schöll, *Eur. Phys. J. Spec. Top.* **191**, 91 (2010).

- [35] S. Lepri, G. Giacomelli, A. Politi, and F. T. Arecchi, *Physica D* **70**, 235 (1994).
- [36] Y. Kuznetsov, *Elements of Applied Bifurcation Theory, Vol. 112 of Applied Mathematical Sciences* (Springer-Verlag, New York, 1995).
- [37] A. F. Ivanov and A. N. Sharkovsky, in *Dynamics Reported, Expositions in Dynamical Systems*, edited by C. K. R. T. Jones, U. Kirchgraber, and H. O. Walther (Springer-Verlag, Berlin, 1992), pp. 165–224.
- [38] M. C. Cross and P. C. Hohenberg, *Rev. Mod. Phys.* **65**, 851 (1993).
- [39] H. Chaté and P. Manneville, *Physica A* **224**, 348 (1996).
- [40] I. Aranson and L. Kramer, *Rev. Mod. Phys.* **74**, 99 (2002).
- [41] R. J. Deissler and K. Kaneko, *Phys. Lett. A* **119**, 397 (1987).
- [42] G. Giacomelli, R. Hegger, A. Politi, and M. Vassalli, *Phys. Rev. Lett.* **85**, 3616 (2000).